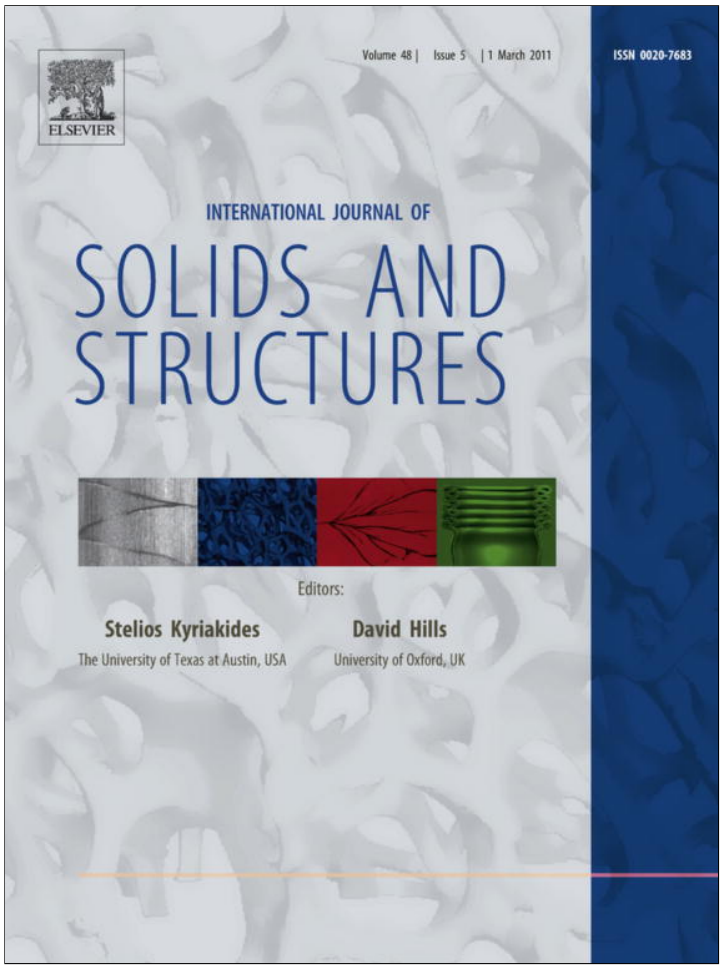

International Journal of Solids and Structures 48 (2011) 648–660

Contents lists available at ScienceDirect

International Journal of Solids and Structures

journal homepage: www.elsevier.com/locate/ijsolstr

Image force on a straight dislocation emitted from a cylindrical void

Vlado A. Lubarda *

Department of Mechanical and Aerospace Engineering, University of California, San Diego, La Jolla, CA 92093-0411, USA
Montenegrin Academy of Sciences and Arts, Rista Stijovića 5, 81000 Podgorica, Montenegro

ARTICLE INFO

Article history:
Received 18 April 2010
Received in revised form 23 August 2010
Available online 05 November 2010

Keywords:
Core energy
Dislocation emission
Interaction energy
Image force
Void

ABSTRACT

The image force exerted by the free surface of a cylindrical circular void on a nearby straight dislocation depends on whether the dislocation has arrived at its location by the emission from the surface of the void, or by the glide from infinity. In the context of elasticity theory, in the first case, the dislocation has been created by imposing the displacement discontinuity along the cut from the free surface of the void to the center of the dislocation, and, in the second case, from the center of the dislocation to infinity. The explicit expressions for the two corresponding image forces are derived and compared. It is shown that the attraction from the free surface of the void is stronger in the first case, particularly for smaller voids. Furthermore, in the case of dislocation emitted from the surface of the void, the interaction energy depends on the cut used to impose the displacement discontinuity, but not in the case of a dislocation approaching the void from infinity. The relevance of the obtained results for the materials science problems is discussed.

1. Introduction

The objective of this paper is to derive the expression for the image force on a straight dislocation emitted from the free surface of a nearby cylindrical void, and evaluate the difference between this force and the image force acting on a dislocation that has arrived near the void from infinity. The two forces are different, because these two dislocations are physically different dislocations, causing different distortions of the material. Speaking in the context of mathematical theory of elasticity, in the case of a dislocation emitted from the surface of the void, the displacement discontinuity is imposed along the cut from the surface of the void to the center of the dislocation, whereas in the second case, the displacement discontinuity is imposed along the cut from infinity to the center of the dislocation. In the context of crystalline elasticity, if the dislocation motion was a glide motion, in the first case the slip took place along the slip plane from the surface of the void to the center of dislocation, and in the second case, from infinity to the center of dislocation. Accordingly, not only the displacement, but the stress and strain fields, and thus the image forces on the dislocation, are different in these two problems. Although such distinction is physically clear and anticipated, as pointed out in the context of the non-uniqueness of solution for a screw dislocation in multiply connected regions by Lubarda (1999),[1] and elaborated upon by Lubarda and Markenscoff (2003), it is desirable to revisit the topic in the context of a general (mixed type) straight dislocation. This particularly so because in recent studies of void growth by emission of dislocations from its free surface (Lubarda et al., 2004; Song et al., 2006; Traiviratana et al., 2008; Meyers et al., 2009), the image force on dislocation was calculated from the interaction energy expression derived by Dundurs and Mura (1964), overlooking the fact that, in their analysis, the displacement discontinuity was imposed from infinity to the center of the dislocation, which means that the dislocation arrived near the void from infinity, rather than being emitted from the surface of the void. Lubarda (2011) subsequently modified this analysis by using the expression for the image force on a dislocation emitted from the surface of the void, but the derivation of this expression, and its comparison with the image force on a dislocation that has arrived from infinity, have not been presented or discussed in that paper. This analysis is presented here. It is shown that the attraction from the void is stronger in the case of a dislocation emitted from the surface of the void than in the case of a dislocation that has approached the void from far away, particularly for smaller voids. This means that in the study of the void growth, the externally applied stress required to emit a dislocation from the surface of the void is greater than earlier reported values, based on a dislocation model with the slip imposed from the dislocation to infinity. On the other hand, the latter model can be used to study a stress driven expansion of a

* Address: Department of Mechanical and Aerospace Engineering, University of California, San Diego, La Jolla, CA 92093-0411, USA. Tel.: +1 858 534 3169; fax: +1 858 534 5698.
E-mail address: vlubarda@ucsd.edu

[1] If the connectivity of the region is n, there are n different solutions, associated with n fundamentally different scenarios of dislocation creation.

0020-7683/$ - see front matter © 2010 Elsevier Ltd. All rights reserved.
doi:10.1016/j.ijsolstr.2010.11.006

pre-existing remote dislocation loop, which consists of a positive and negative dislocation on the same slip plane, during which one dislocation is driven away from the loop and the other toward the loop.[2] In this case, the expanding loop can be considered to be a superposition of two distant dislocations created by opposite slips from their centers to either infinity, or to the surface of the void.

If a dislocation is in a close proximity of a very large void, the image forces are nearly the same, regardless of whether dislocation was emitted from the surface of the void, or it has arrived there from infinity. This is because the dislocation is then not able to recognize a large radius of the void, and behaves as if it were near a straight boundary of a semi-infinite (simply-connected) domain (Head, 1953). Furthermore, we show that the interaction energy of a dislocation emitted from the surface of the void depends on the cut used to impose the displacement discontinuity, which is not so in the case of a dislocation that has approached the void from infinity. The performed energy analysis required a careful incorporation of the dislocation core energy, which depends on the selected cut along which the displacement discontinuity is imposed (Gavazza and Barnett, 1976). This is reminiscent to the incorporation of the core energy in the mechanics of strain relaxation of thin films, when different cuts are used to impose the displacement discontinuity from the dislocation at the interface of the substrate and a thin film to the free surface of the film (Lubarda, 1997, 1998).

We note that the analysis presented in this paper is based on the Volterra dislocation model and linear elasticity. For this to reasonably apply, we assume that the radius of the void is at least 10 times greater than the magnitude of the Burgers vector of the dislocation. Otherwise, the ledge left on the surface of the void by the emission of dislocation would appreciably distort the circular geometry of the void, which is assumed to hold in the considered boundary value problem of linear elasticity. In addition, a dislocation is assumed to be fully formed and therefore sufficiently away from the surface of the void, perhaps by at least two lengths of its Burgers vector. An incomplete or incipient dislocation, dominated by its heavily distorted core, would otherwise reside near the surface of the void, requiring the other type of analysis, such as that based on the Peierls semi-discrete model of lattice dislocation, or the atomistic calculations.[3]

2. Stress functions for the straight dislocation near a cylindrical void

2.1. Dislocation approaching the void from infinity

Consider a straight dislocation with the Burgers vector $\mathbf{b} = \{b_x, b_y, b_z\}$ near a cylindrical circular void of radius a, at the distance $\overline{OA} = \alpha a\,(\alpha > 1)$ from the center of the void (Fig. 1).[4] If the dislocation has arrived near the void from infinity, i.e., if it is (from the standpoint of elasticity theory) created by imposing the displacement discontinuity along a cut from A to infinity, for example along the x-axis, Dundurs and Mura (1964) have shown that the stress functions for the edge dislocation components b_x and b_y are, respectively:

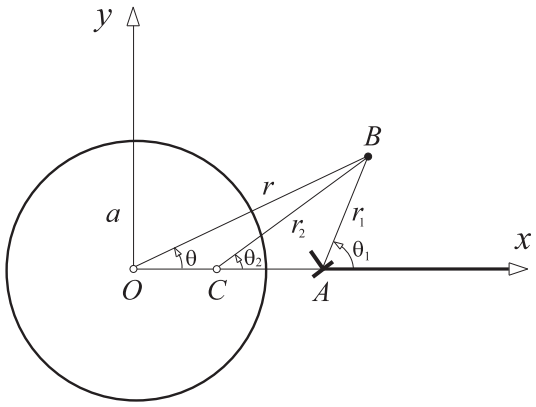

Fig. 1. The radii r, r_1, r_2 and the angles θ, θ_1, θ_2 appearing in the expressions for the stress and displacement components at the point B due to straight dislocation at the point A. The radius of the void is a, and the lengths $\overline{OA} = \alpha a$ and $\overline{OC} = a/\alpha$. The dislocation is created by the displacement discontinuity along the x-axis from A to infinity.

$$\Phi^{b_x} = -\frac{Gb_x}{2\pi(1-\nu)}\Big[r_1 \ln r_1 \sin\theta_1 - r_2 \ln r_2 \sin\theta_2 + r \ln r \sin\theta + \frac{a^2}{2r}\sin\theta + \frac{\alpha^2-1}{2\alpha^3}\, a\left(\sin 2\theta_2 - \frac{\alpha^2-1}{\alpha}\,\frac{a}{r_2}\sin\theta_2\right)\Big], \tag{1}$$

$$\Phi^{b_y} = \frac{Gb_y}{2\pi(1-\nu)}\Big[r_1 \ln r_1 \cos\theta_1 - r_2 \ln r_2 \cos\theta_2 + r \ln r \cos\theta + \frac{a^2}{2r}\cos\theta - \frac{\alpha^2-1}{2\alpha^3}\, a\left(\cos 2\theta_2 - \frac{\alpha^2-1}{\alpha}\,\frac{a}{r_2}\cos\theta_2 + 2\alpha^2 \ln\frac{r}{r_2}\right)\Big]. \tag{2}$$

The shear modulus and Poisson's ratio of the material are G and ν. The complete Airy stress function is $\Phi = \Phi^{b_x} + \Phi^{b_y}$, and

$$\sigma_x = \frac{\partial^2 \Phi}{\partial y^2}, \quad \sigma_y = \frac{\partial^2 \Phi}{\partial x^2}, \quad \sigma_{xy} = -\frac{\partial^2 \Phi}{\partial x \partial y}. \tag{3}$$

The explicit stress and displacement components are the sums of the corresponding expressions listed in the Appendices A and B. For the displacement expressions, the angle range to be applied is $0 \leqslant (\theta, \theta_1, \theta_2) \leqslant 2\pi$, so that the displacement discontinuity is imposed from the center of the dislocation to infinity along the positive x-axis. The Burgers circuit around the dislocation gives the Burgers vector $\mathbf{b}$, regardless of whether the circuit encompasses the void or not.

The stress function associated with the out-of-plane stresses is

$$\varphi = -\frac{Gb_z}{2\pi} \ln\frac{r r_1}{a r_2}, \tag{4}$$

such that:

$$\sigma_{zx} = \frac{\partial \varphi}{\partial y}, \quad \sigma_{zy} = -\frac{\partial \varphi}{\partial x}. \tag{5}$$

The explicit out-of-plane stresses and the displacement expressions are also the sums of the corresponding expressions listed in the Appendices A and B.

2.2. Dislocation exited at the surface of the void

If the dislocation, arriving from infinity, has exited the material at the free surface of the void (Fig. 2), leaving behind a uniform step discontinuity (b_x, b_y, b_z) from the surface of the void to infinity, the Airy stress functions are obtained from (1) and (2) by taking $\theta_1 = \theta_2$, which gives:

[2] If the dislocation nearer to the void exits at the surface of the void, the slip step is there created. When many dislocations are considered, on parallel and intersecting slip planes in a high dislocation density region around a micron or larger size void, the net effect can be the void growth under tensile, or void collapse under compressive loading. A study of such process within the framework of discrete dislocation dynamics has been recently conducted by Segurado and Llorca (2009), who also give the reference to earlier related work.

[3] The first molecular dynamics studies of the dislocation emission from the surface of voids were reported by Belak (1998), Rudd and Belak (2002), and Moriarty et al. (2002). The reference to subsequent work can be found in Rudd (2009), Bulatov et al. (2010), and Bringa et al. (2010).

[4] The elastic field of a prismatic-dislocation loop near a spherical void, and the attraction of the loop by the surface of the void, have been studied by Willis and Bullough (1971), Wolfer and Drugan (1988), and Ahn et al. (2006).

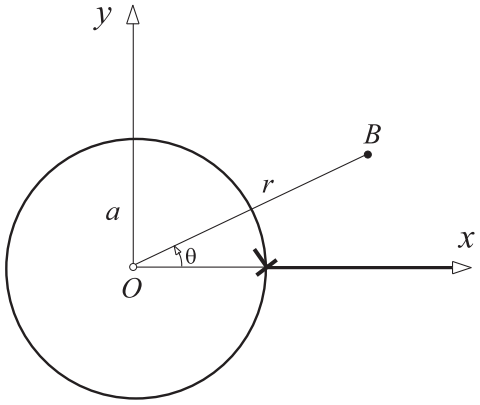

Fig. 2. If the dislocation from Fig. 1 exits at the surface of the void, a uniform step discontinuity (b_x, b_y, b_z) is left behind it along the x-axis from the surface of the void to infinity.

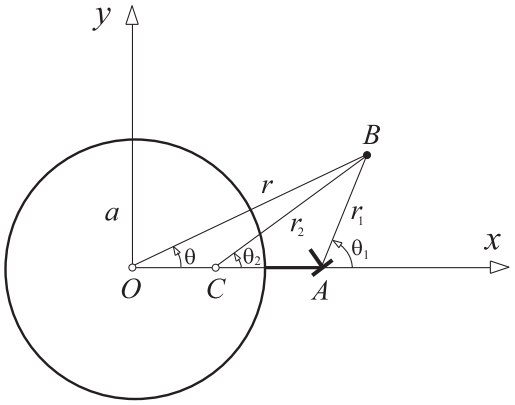

Fig. 3. The dislocation at the point A created by imposing the displacement discontinuity along the cut from the surface of the void to the center of the dislocation. When B is on the boundary of the void, $r_1\sin\theta_1 = r_2\sin\theta_2 = a\sin\theta$, $r_1 = \alpha r_2$, and $\theta_2 = \theta + (\pi - \theta_1)$.

$$\Phi^{b_x} = -\frac{Gb_x}{2\pi(1-\nu)}\left(r\ln r + \frac{a^2}{2r}\right)\sin\theta, \tag{6}$$

$$\Phi^{b_y} = \frac{Gb_y}{2\pi(1-\nu)}\left(r\ln r + \frac{a^2}{2r}\right)\cos\theta. \tag{7}$$

The stress function for the out-of-plane stresses is

$$\varphi = -\frac{Gb_z}{2\pi}\ln\frac{r}{a}, \tag{8}$$

as if the screw dislocation was placed at O in an infinite medium. The corresponding stress and displacement components are listed in Appendix A.

2.3. Dislocation emitted from the surface of the void

If the dislocation has been emitted from the surface of the void, so that the displacement discontinuity is created along the cut from the void surface to the center of the dislocation (Fig. 3), the Airy stress functions for the two edge dislocation components are obtained by subtracting the Airy stress functions corresponding to dislocations in Figs. 1 and 2. This superposition, sketched in Fig. 4, gives:

$$\Phi^{b_x} = -\frac{Gb_x}{2\pi(1-\nu)}\Big[r_1\ln r_1\sin\theta_1 - r_2\ln r_2\sin\theta_2 + \frac{\alpha^2-1}{2\alpha^3}\,a\left(\sin 2\theta_2 - \frac{\alpha^2-1}{\alpha}\,\frac{a}{r_2}\sin\theta_2\right)\Big], \tag{9}$$

$$\Phi^{b_y} = \frac{Gb_y}{2\pi(1-\nu)}\Big[r_1\ln r_1\cos\theta_1 - r_2\ln r_2\cos\theta_2 - \frac{\alpha^2-1}{2\alpha^3}\,a\left(\cos 2\theta_2 - \frac{\alpha^2-1}{\alpha}\,\frac{a}{r_2}\cos\theta_2 + 2\alpha^2\ln\frac{r}{r_2}\right)\Big]. \tag{10}$$

The stress function associated with the out-of-plane stresses is

$$\varphi = -\frac{Gb_z}{2\pi}\ln\frac{r_1}{r_2}. \tag{11}$$

The explicit stress and displacement components are listed in Appendix B. They are constructed by using a helpful table from Dundurs and Mura (1964), also listed in Asaro and Lubarda (2006), which relates the biharmonic contributions to the Airy stress function with the corresponding stress and displacement components. In the displacement expressions, the angle range to be applied is $-\pi \leqslant (\theta_1, \theta_2) \leqslant \pi$, so that the displacement discontinuity is imposed from the surface of the void to the center of dislocation along the x-axis. The Burgers circuit around the dislocation gives the Burgers vector **b**, if the circuit does not encompass the void.

3. Image force on a dislocation

The free surface of the void exerts an attractive force on a nearby dislocation. This can be calculated either directly from the Peach–Koehler expression for the dislocation force, or from the gradient of the interaction energy (as done in Section 4). The Peach–Koehler force on a straight dislocation is (Hirth and Lothe, 1982):

$$\mathbf{F} = (\boldsymbol{\sigma}\cdot\mathbf{b})\times\mathbf{e}_z, \tag{12}$$

where $\boldsymbol{\sigma}$ is the stress tensor at the center of the dislocation due to a nonsingular image field induced on a dislocation by the free surface of the void, and $\mathbf{e}_z$ is the unit vector along the dislocation line. The z-component of the image force vanishes ($F_z = 0$), while the x and y-components are

$$F_x = \sigma_{yx}b_x + \sigma_y b_y + \sigma_{yz}b_z, \quad F_y = -\left(\sigma_x b_x + \sigma_{xy}b_y + \sigma_{xz}b_z\right). \tag{13}$$

The glide and climb force components are

$$F_\rho = \sigma_{n\rho}b_\rho + \sigma_{nz}b_z, \quad F_n = -\left(\sigma_\rho b_\rho + \sigma_{\rho z}b_z\right), \tag{14}$$

where $b_\rho = (b_x^2 + b_y^2)^{1/2}$ is the edge component of the dislocation along the slip direction ρ, and n designates the direction orthogonal to the slip plane.

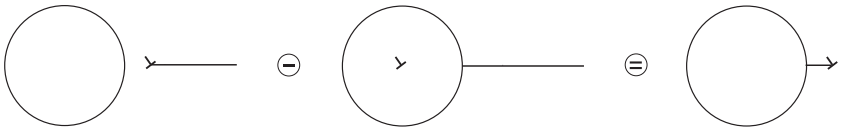

Fig. 4. Superposition principle used to construct the solution for a dislocation emitted from the surface of the void.

3.1. Image force on a dislocation created by cut 1

If the dislocation is created by cut 1, as shown in Fig. 1, the image stress components at the center of the dislocation are

$$\begin{aligned}\sigma_x &= \frac{Gb_y}{2\pi(1-\nu)}\,\frac{a^2}{x(x^2-a^2)},\\ \sigma_y &= -\frac{Gb_y}{2\pi(1-\nu)}\,\frac{a^2}{x(x^2-a^2)},\\ \sigma_{xy} &= -\frac{Gb_x}{2\pi(1-\nu)}\,\frac{a^2(2x^2-a^2)}{x^3(x^2-a^2)},\\ \sigma_{yz} &= -\frac{Gb_z}{2\pi}\,\frac{a^2}{x(x^2-a^2)}, \quad \sigma_{xz}=0.\end{aligned} \tag{15}$$

Upon the substitution of (15) into (13), there follows:

$$F_x = -\frac{G}{2\pi(1-\nu)}\,\frac{a^2}{x(x^2-a^2)}\left[\left(2-\frac{a^2}{x^2}\right)b_x^2 + b_y^2 + (1-\nu)b_z^2\right], \tag{16}$$

$$F_y = \frac{Gb_xb_y}{2\pi(1-\nu)}\,\frac{a^2}{x^3}. \tag{17}$$

The glide and climb force components, along the edge component of the Burgers vector $\mathbf{b}_\rho = \{b_x, b_y\}$, and orthogonal to it, can be calculated from:

$$F_\rho = F_x\cos\vartheta_o + F_y\sin\vartheta_0, \quad F_n = F_y\cos\vartheta_0 - F_x\sin\vartheta_0, \tag{18}$$

where $\tan\vartheta_0 = b_y/b_x$. The substitution of (16) and (17) into (18) gives:

$$F_\rho = -\frac{G}{2\pi(1-\nu)}\,\frac{a^2\cos\vartheta_0}{x(x^2-a^2)}\left\{\left[2-\frac{a^2}{x^2}-2\left(1-\frac{a^2}{x^2}\right)\sin^2\vartheta_0\right](b_x^2+b_y^2) + (1-\nu)b_z^2\right\}, \tag{19}$$

$$F_n = \frac{G}{2\pi(1-\nu)}\,\frac{a^2\sin\vartheta_0}{x(x^2-a^2)}\left\{\left[1+2\left(1-\frac{a^2}{x^2}\right)\cos^2\vartheta_0\right](b_x^2+b_y^2) + (1-\nu)b_z^2\right\}. \tag{20}$$

3.2. Image force on a dislocation created by cut 2

If the dislocation is created by cut 2 (Fig. 3), the image stress components at the center of the dislocation are

$$\begin{aligned}\sigma_x &= \frac{Gb_y}{2\pi(1-\nu)}\,\frac{x}{x^2-a^2}\left[\frac{a^2}{x^2}-\left(1-\frac{a^2}{x^2}\right)^2\right],\\ \sigma_y &= -\frac{Gb_y}{2\pi(1-\nu)}\,\frac{x}{x^2-a^2}\left(1+\frac{a^2}{x^2}-\frac{a^4}{x^4}\right),\\ \sigma_{xy} &= -\frac{Gb_x}{2\pi(1-\nu)}\,\frac{x}{x^2-a^2},\\ \sigma_{yz} &= -\frac{Gb_z}{2\pi}\,\frac{x}{x^2-a^2}, \quad \sigma_{xz}=0.\end{aligned} \tag{21}$$

Upon the substitution of (21) into (13), the horizontal and vertical components of the image force are found to be:

$$F_x = -\frac{G}{2\pi(1-\nu)}\,\frac{x}{x^2-a^2}\left[b_x^2 + \left(1+\frac{a^2}{x^2}-\frac{a^4}{x^4}\right)b_y^2 + (1-\nu)b_z^2\right], \tag{22}$$

$$F_y = \frac{Gb_xb_y}{2\pi(1-\nu)}\,\frac{1}{x}\left(2-\frac{a^2}{x^2}\right). \tag{23}$$

The corresponding glide and climb forces are

$$F_\rho = -\frac{G}{2\pi(1-\nu)}\,\frac{x\cos\vartheta_0}{x^2-a^2}\left\{\left[1-2\left(1-\frac{a^2}{x^2}\right)^2\sin^2\vartheta_0\right](b_x^2+b_y^2) + (1-\nu)b_z^2\right\}, \tag{24}$$

$$F_n = \frac{G}{2\pi(1-\nu)}\,\frac{x\sin\vartheta_0}{x^2-a^2}\left\{\left[1+\frac{a^2}{x^2}-\frac{a^4}{x^4}+2\left(1-\frac{a^2}{x^2}\right)^2\cos^2\vartheta_0\right](b_x^2+b_y^2) + (1-\nu)b_z^2\right\}. \tag{25}$$

3.3. Comparison of image forces

If a dislocation is pure edge with the Burgers vector parallel to the x or y-axis, the differences in the dislocation image forces corresponding to two cuts are, respectively:

$$F_x^{(1)} - F_x^{(2)} = \sigma_{xy}^A(x,0)b_x = \frac{Gb_x^2}{2\pi(1-\nu)}\,\frac{1}{x}\left(1-\frac{a^2}{x^2}\right), \tag{26}$$

$$F_x^{(1)} - F_x^{(2)} = \sigma_y^A(x,0)b_y = \frac{Gb_y^2}{2\pi(1-\nu)}\,\frac{1}{x}\left(1+\frac{a^2}{x^2}\right), \tag{27}$$

where $\sigma_{xy}^A(x,0)$ and $\sigma_y^A(x,0)$ are the in-plane shear and normal stresses along the x-axis of the auxiliary problem considered in Appendix A (Fig. 5). In the case of pure screw, the difference in the image forces is

$$F_x^{(1)} - F_x^{(2)} = \sigma_{zy}^A(x,0)b_z = \frac{Gb_z^2}{2\pi}\,\frac{1}{x}, \tag{28}$$

where $\sigma_{zy}^A(x,0)$ is the out-of-plane shear stress along the x-axis of the auxiliary problem from Appendix A.

3.4. Relationship to dislocation inside a circular cylinder

There are similarities in the solution for the dislocation emitted from the surface of a cylindrical void and for the dislocation inside a solid circular cylinder. For example, if the edge dislocation with the Burgers vector b_x is inside a circular cylinder, on the x-axis at $x = \beta a$ $(0 < \beta < 1)$, it is pulled toward the free surface by the force (Dundurs and Sendeckyj, 1965):

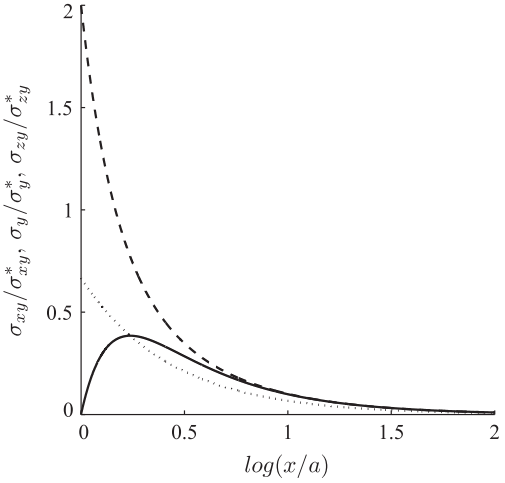

Fig. 5. The shear and normal stresses along the x-axis of the auxiliary problem from Appendix A. The normalizing stress factors are $\sigma_{xy}^* = G^*(b_x/a)$ (solid curve), $\sigma_y^* = G^*(b_y/a)$ (dashed curve) and $\sigma_{zy}^* = G^*(b_z/a)$, where $G^* = G/[2\pi(1-\nu)]$ (dotted curve).

$$F_x^{\text{cyl}} = \frac{Gb_x^2/a}{2\pi(1-\nu)}\,\frac{\beta}{1-\beta^2}. \tag{29}$$

On the other hand, if the edge dislocation with the Burgers vector b_x is outside a cylindrical void, on the x-axis at $x = \alpha a$ ($\alpha > 1$), it is under the force:

$$F_x^{\text{void}} = -\frac{Gb_x^2/a}{2\pi(1-\nu)}\,\frac{\alpha}{\alpha^2-1}. \tag{30}$$

The transition between the above two expressions is made by the substitution $\alpha = 1/\beta$.

No such simple correspondence exists for the edge dislocation with the Burgers vector b_y, since then:

$$F_x^{\text{cyl}} = \frac{Gb_y^2/a}{2\pi(1-\nu)}\,\frac{\beta^3}{1-\beta^2},$$

$$F_x^{\text{void}} = -\frac{Gb_y^2/a}{2\pi(1-\nu)}\,\frac{\alpha}{\alpha^2-1}\left(1+\frac{1}{\alpha^2}-\frac{1}{\alpha^4}\right).$$

As a matter of fact, a closer inspection of the Airy stress functions, for the dislocation in a solid cylinder and in an infinite matrix near the void, reveals that the structures of Φ^{b_x} are equivalent, but not of Φ^{b_y}; cf. (7) of Dundurs and Sendeckyj (1965) with (10) here. Of course, the solutions for the pure screw dislocation are equivalent, because both are obtained by the superposition of the fields from two opposite screw dislocations placed at two points conjugate to each other with respect to the boundary $r = a$.

4. Interaction energy

The elastic strain energy per unit dislocation length within a large cylinder of radius $R \gg \alpha a$ around the void, excluding the dislocation core energy,[5] can be expressed by the Gauss divergence theorem as

$$E = U + E_R + E_c, \tag{31}$$

where E_R is the work done by tractions acting over the remote boundary on the corresponding displacements, and E_c is the work done by tractions acting over the core surface of small radius c, i.e.,

$$E_c = -\frac{1}{2}\oint (\sigma_r u_r + \sigma_{r\theta}u_\theta)c\ \mathrm{d}\theta,$$

$$E_R = \frac{1}{2}\oint (\sigma_r u_r + \sigma_{r\theta}u_\theta)R\ \mathrm{d}\theta. \tag{32}$$

For a sufficiently small core radius c, the stress field associated with a dislocation in an infinite medium (self dislocation field) dominates over the image stress contributions, and the work E_c can be conveniently calculated from the stress and displacement fields of an isolated dislocation in an infinite medium.[6] In the case of the horizontal cut (along the x-axis) this is (e.g., Lubarda, 1997):

$$E_c = -\frac{G}{8\pi(1-\nu)}\left[b_x^2 - b_y^2 - \frac{1}{2(1-\nu)}\,(b_x^2+b_y^2)\right]. \tag{33}$$

In the case of cut 1, the energy contribution E_R can be conveniently calculated by using the stress and displacement fields from Appendix A, because the small distance $(\alpha-1)a \ll R$ is not observed at a far remote contour R. In fact, at a far remote contour ($R \gg a$), the radius of the void is not observed either, so that E_R can be calculated from the stress and displacement fields of a dislocation in an infinite medium, which gives $E_R = -E_c$. In the case of cut 2, the displacement discontinuity from the surface of the void to nearby dislocation is not observed at a far remote contour R at all, so that in this case $E_R = 0$.[7]

The energy contribution U, referred to as the interaction energy, is equal to the work done by tractions on the displacement discontinuity along the cut used to create a dislocation. This will be evaluated for utilized cuts in the sequel. Since an infinitesimal variation of the dislocation position (δx) does not affect E_c and E_R, the x-component of the image force can be calculated as

$$F_x = -\frac{\partial U}{\partial x}. \tag{34}$$

4.1. Interaction energy for a dislocation created by cut 1

The interaction energy for a dislocation created by a cut from the dislocation to $R \to \infty$, along the positive x-axis, is

$$U = \frac{1}{2}b_x\int_{\alpha a+c}^{R}\sigma_{xy}(x,0)\mathrm{d}x + \frac{1}{2}b_y\int_{\alpha a+c}^{R}\sigma_y(x,0)\mathrm{d}x + \frac{1}{2}b_z\int_{\alpha a+c}^{R}\sigma_{yz}(x,0)\mathrm{d}x. \tag{35}$$

By substituting the stress expressions and integrating, the α-dependent part[8] of the interaction energy (relevant for the image force calculation) is

$$U = \frac{G}{4\pi(1-\nu)}\left\{\left[b_x^2+b_y^2+(1-\nu)b_z^2\right]\ln\frac{\alpha^2-1}{\alpha^2} - b_x^2\,\frac{1}{\alpha^2}\right\}, \tag{36}$$

or, in terms of $x = \alpha a$:

$$U = \frac{G}{4\pi(1-\nu)}\left\{\left[b_x^2+b_y^2+(1-\nu)b_z^2\right]\ln\left(1-\frac{a^2}{x^2}\right) - b_x^2\,\frac{a^2}{x^2}\right\}. \tag{37}$$

By substituting (37) into (34), the horizontal component of the dislocation force is found to be as given by (16).

Alternatively, to circumvent the integration, the interaction energy can be calculated from (35) by substituting the stress expressions in terms of the derivatives of the stress functions Φ and φ (Dundurs, 1969; Eshelby, 1979). It readily follows that:

$$U = \frac{1}{2}\,b_x\left[\frac{\partial\Phi}{\partial y}(\alpha a+c,0) - \frac{\partial\Phi}{\partial y}(R,0)\right] - \frac{1}{2}\,b_y\left[\frac{\partial\Phi}{\partial x}(\alpha a+c,0) - \frac{\partial\Phi}{\partial x}(R,0)\right] + \frac{1}{2}\,b_z[\varphi(\alpha a+c,0) - \varphi(R,0)],$$

which reproduces (37).

4.2. Interaction energy for a dislocation created by cut 2

The interaction energy for a dislocation created by a cut from the free surface to the dislocation, along the x-axis, is

[5] The severe distortion of material within the core region associated with the constant displacement discontinuity from the center of the core gives rise to singular stress and strain fields within the core. This divergence can be eliminated by using either non-linear or non-local elasticity models, or semi-discrete and atomistic models (Tadmor et al., 1996; Rudd, 2009).

[6] If a dislocation is very close to the surface of the void, the Peierls dislocation model should be used, although there is no closed form analytical solution for such dislocation near a cylindrical void. An analytical study of the dislocation nucleation from a crack tip with the Peierls type model was given by Rice (1992).

[7] The effects of couple stresses on dislocation strain energy are considered by Lubarda (2003).

[8] In an infinite medium, the interaction energy is formally infinite, but the divergent term

$$\frac{G}{4\pi(1-\nu)}\left[b_x^2+b_y^2+(1-\nu)b_z^2\right]\ln\frac{R}{c},$$

omitted in (36) and (37), does not depend on the dislocation position and does not contribute to the dislocation image force.

$$U = -\frac{1}{2}b_x\int_a^{\alpha a-c}\sigma_{xy}(x,0)\mathrm{d}x - \frac{1}{2}b_y\int_a^{\alpha a-c}\sigma_y(x,0)\mathrm{d}x - \frac{1}{2}b_z\int_a^{\alpha a-c}\sigma_{yz}(x,0)\mathrm{d}x. \tag{38}$$

By substituting the stress expressions from Appendix B and integrating, the relevant portion[9] of the interaction energy is found to be:

$$U = \frac{G}{4\pi(1-\nu)}\left\{\left[b_x^2+b_y^2+(1-\nu)b_z^2\right]\ln(\alpha^2-1) - b_y^2\,\frac{1}{\alpha^2} - \frac{1}{2}\left(b_x^2-b_y^2\right)\right\}, \tag{39}$$

or, in terms of $x = \alpha a$:

$$U = \frac{G}{4\pi(1-\nu)}\left\{\left[b_x^2+b_y^2+(1-\nu)b_z^2\right]\ln\left(\frac{x^2}{a^2}-1\right) - b_y^2\,\frac{a^2}{x^2} - \frac{1}{2}\left(b_x^2-b_y^2\right)\right\}. \tag{40}$$

The constant term proportional to $(b_x^2 - b_y^2)$ is retained in (39) and (40), because it plays an important role in the energy analysis presented in Section 5, which addresses the dislocation glide along an inclined slip plane, with the displacement discontinuity imposed along that direction.

Alternatively, (40) can be deduced from:

$$U = \frac{1}{2}\,b_x\left[\frac{\partial\Phi}{\partial y}(\alpha a-c,0) - \frac{\partial\Phi}{\partial y}(a,0)\right] - \frac{1}{2}\,b_y\left[\frac{\partial\Phi}{\partial x}(\alpha a-c,0) - \frac{\partial\Phi}{\partial x}(a,0)\right] + \frac{1}{2}\,b_z[\varphi(\alpha a-c,0) - \varphi(a,0)].$$

The substitution of this expression into $F_x = -\partial U/\partial x$ reproduces (22).

5. Dislocation on an inclined slip plane

In the study of void growth by dislocation emission from the surface of the void (Lubarda, 2011), the dislocation is emitted from a particular point on the surface of the void, and at an angle relative to the loading direction, which make the emission of dislocation most favorable. For this study, it is necessary to consider a dislocation in the configuration shown in Fig. 6, where the horizontal and vertical directions (x_0, y_0) correspond to the external (biaxial) loading directions, and ξ is the slip direction. The slip direction intersects the surface of the void at the point specified by the angle ψ_0, while the slip plane orientation is specified by the angle ω_0. At the position shown in Fig. 6, the dislocation is at a distance ρ, measured along the ξ-direction from the surface of the void. The corresponding distance r from the center of the void, and the angle ϑ, are

$$r^2 = a^2+\rho^2+2a\rho\cos\omega_0, \quad \sin\vartheta = \frac{a}{r}\,\sin\omega_0. \tag{41}$$

For later purposes, we also note that $\mathrm{d}r/\mathrm{d}\rho = \cos\vartheta$ and $\mathrm{d}\vartheta/\mathrm{d}\rho = -(\sin\vartheta)/r$.

5.1. Image forces corresponding to cut 1

Consider first the case when the dislocation arrived at the position shown in Fig. 6 by glide from infinity (under externally applied stress). The components of the image force exerted by the surface of the void in this case can be written down directly from the expressions (19) and (20), by replacing x with r, and ϑ_0 with ϑ. Since $b_x = b_\rho\cos\vartheta$ and $b_y = b_\rho\sin\vartheta$, there follows[10]:

$$F_\rho = -\frac{G}{2\pi(1-\nu)}\,\frac{a^2\cos\vartheta}{r(r^2-a^2)}\left\{\left[2-\frac{a^2}{r^2}-2\,\frac{a^2}{r^2}\left(1-\frac{a^2}{r^2}\right)\sin^2\omega_0\right]b_\rho^2 + (1-\nu)b_z^2\right\}, \tag{42}$$

$$F_n = \frac{G}{2\pi(1-\nu)}\,\frac{a^3\sin\omega_0}{r^2(r^2-a^2)}\left\{\left[3-2\,\frac{a^2}{r^2}-2\,\frac{a^2}{r^2}\left(1-\frac{a^2}{r^2}\right)\sin^2\omega_0\right]b_\rho^2 + (1-\nu)b_z^2\right\}, \tag{43}$$

where $\cos\vartheta = [1-(a^2/r^2)\sin^2\omega_0]^{1/2}$.

The corresponding interaction energy can be deduced from (37) as

$$U = \frac{G}{4\pi(1-\nu)}\left\{\left[b_\rho^2+(1-\nu)b_z^2\right]\ln\left(1-\frac{a^2}{r^2}\right) - b_\rho^2\,\frac{a^2}{r^2}\left(1-\frac{a^2}{r^2}\sin^2\omega_0\right)\right\}. \tag{44}$$

This reproduces the glide force by $F_\rho = -\partial U/\partial\rho$, because the strain energy is equal to the interaction energy ($E_c + E_R = 0$ and $E = U$).

If the dislocation is pure edge with the Burgers vector of magnitude b, (44) reduces to:

$$U = \frac{Gb^2}{4\pi(1-\nu)}\left[\ln\left(1-\frac{a^2}{r^2}\right) - \frac{a^2}{r^2}\left(1-\frac{a^2}{r^2}\,\sin^2\omega_0\right)\right], \tag{45}$$

in agreement with the expression (7.7) from Dundurs (1969), while (42) and (43) become:

$$F_\rho = -\frac{Gb^2}{2\pi(1-\nu)}\,\frac{a^2\cos\vartheta}{r(r^2-a^2)}\left[2-\frac{a^2}{r^2}-2\,\frac{a^2}{r^2}\left(1-\frac{a^2}{r^2}\right)\sin^2\omega_0\right], \tag{46}$$

$$F_n = \frac{Gb^2}{2\pi(1-\nu)}\,\frac{a^3\sin\omega_0}{r^2(r^2-a^2)}\left[3-2\,\frac{a^2}{r^2}-2\,\frac{a^2}{r^2}\left(1-\frac{a^2}{r^2}\right)\sin^2\omega_0\right]. \tag{47}$$

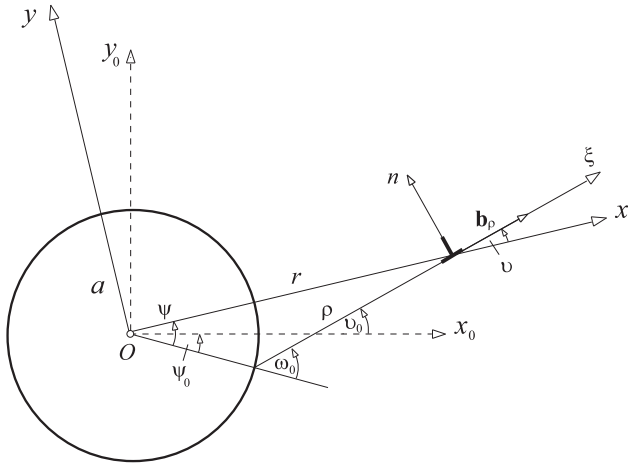

Fig. 6. A dislocation with its edge component along the slip direction ξ, whose orientation is specified by the angle ω_0. The slip direction intersects the surface of the void at the point defined by the angle ψ_0. As the dislocation glides away from the void and the distance ρ increases, the angle ϑ decreases from ω_0 to 0.

[9] The c-dependent term, not contributing to the dislocation force,

$$\frac{G}{4\pi(1-\nu)}\left[b_x^2+b_y^2+(1-\nu)b_z^2\right]\ln\frac{a}{c},$$

is omitted in (39) and (40).

[10] To use the results from Section 4 directly, we consider that at each new position of dislocation along its slip plane, the new x-direction is passed through O and the center of the dislocation, along which the displacement discontinuity is imposed from the dislocation to infinity.

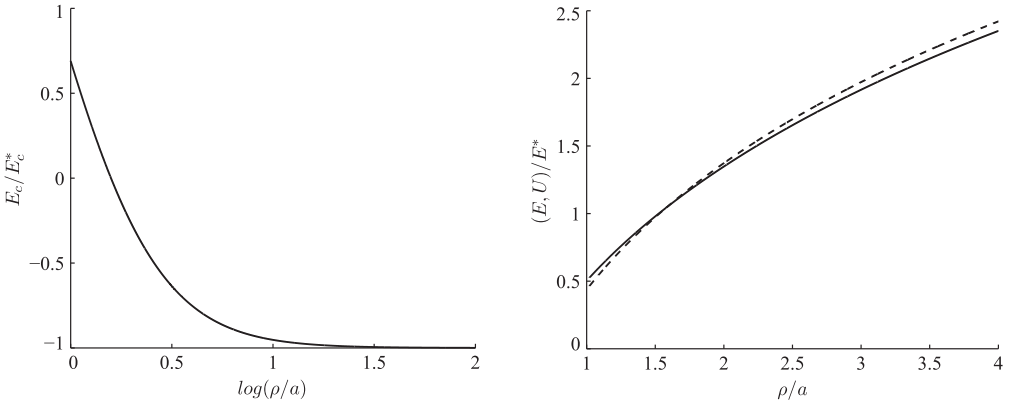

Fig. 7. (a) The variation of the core energy (52) with the distance ρ. The normalizing factor is $E_c^* = \mathbb{E}_c$, given by Eq. (60), which is also the limiting value of E_c as $\rho \to \infty$. (b) The variation of the interaction energy U (dashed curve) from (50), and the strain energy E (solid curve) from (54). The normalizing energy factor is $E^* = Gb^2/[4\pi(1-\nu)]$.

5.2. Image forces corresponding to cut 2

If the dislocation in Fig. 6 has been emitted from the surface of the void (under externally applied stress), the components of the image force are recognized, from (24) and (25), to be:

$$F_\rho = -\frac{G}{2\pi(1-\nu)}\frac{r\cos\vartheta}{r^2-a^2}\left\{\left[1-2\frac{a^2}{r^2}\left(1-\frac{a^2}{r^2}\right)^2\sin^2\omega_0\right]b_\rho^2+(1-\nu)b_z^2\right\}, \tag{48}$$

$$F_n = \frac{G}{2\pi(1-\nu)}\frac{a\sin\omega_0}{r^2-a^2}\left\{\left[3\left(1-\frac{a^2}{r^2}\right)+\frac{a^4}{r^4} - 2\frac{a^2}{r^2}\left(1-\frac{a^2}{r^2}\right)^2\sin^2\omega_0\right]b_\rho^2+(1-\nu)b_z^2\right\}. \tag{49}$$

The corresponding interaction energy follows from (40):

$$U = \frac{G}{4\pi(1-\nu)}\left\{\left[b_\rho^2+(1-\nu)b_z^2\right]\ln\left(\frac{r^2}{a^2}-1\right) + b_\rho^2\left[\frac{a^2}{r^2}\left(1-\frac{a^2}{r^2}\right)\sin^2\omega_0-\frac{1}{2}\right]\right\}. \tag{50}$$

The dislocation core energy is obtained from (33) by substituting $b_x = b_\rho\cos\vartheta$ and $b_y = b_\rho\sin\vartheta$, which gives (e.g., Lubarda, 2006):

$$E_c = -\frac{Gb_\rho^2}{8\pi(1-\nu)}\left[\cos 2\vartheta-\frac{1}{2(1-\nu)}\right], \tag{51}$$

or, in terms of r:

$$E_c = \frac{Gb_\rho^2}{4\pi(1-\nu)}\left[\frac{a^2}{r^2}\sin^2\omega_0-\frac{1-2\nu}{4(1-\nu)}\right]. \tag{52}$$

As the dislocation glides along the slip plane, the angle ϑ changes, and so does the core energy (Fig. 7(a)). Consequently, in this case the glide force on the dislocation is determined from the gradient of the strain energy:

$$F_\rho = -\frac{\partial E}{\partial\rho}, \tag{53}$$

where

$$E = U + E_c = \frac{G}{4\pi(1-\nu)}\left\{\left[b_\rho^2+(1-\nu)b_z^2\right]\ln\left(\frac{r^2}{a^2}-1\right) + b_\rho^2\left[\frac{a^2}{r^2}\left(2-\frac{a^2}{r^2}\right)\sin^2\omega_0-\frac{3-4\nu}{4(1-\nu)}\right]\right\}. \tag{54}$$

The variations of E and U with ρ are shown in Fig. 7(b). The negative of the slope of E, not U, is the glide force F_ρ. It can be easily verified that (53) with (54) reproduces (48).

If the dislocation is a pure edge, (50) reduces to:

$$U = \frac{Gb^2}{4\pi(1-\nu)}\left[\ln\left(\frac{r^2}{a^2}-1\right)+\frac{a^2}{r^2}\left(1-\frac{a^2}{r^2}\right)\sin^2\omega_0-\frac{1}{2}\right], \tag{55}$$

while (54) becomes:

$$E = \frac{Gb^2}{4\pi(1-\nu)}\left[\ln\left(\frac{r^2}{a^2}-1\right)+\frac{a^2}{r^2}\left(2-\frac{a^2}{r^2}\right)\sin^2\omega_0-\frac{3-4\nu}{4(1-\nu)}\right]. \tag{56}$$

The Eqs. (48) and (49) for the glide and climb forces in this case are

$$F_\rho = -\frac{Gb^2}{2\pi(1-\nu)}\frac{r\cos\vartheta}{r^2-a^2}\left[1-2\frac{a^2}{r^2}\left(1-\frac{a^2}{r^2}\right)^2\sin^2\omega_0\right], \tag{57}$$

$$F_n = \frac{Gb^2}{2\pi(1-\nu)}\frac{a\sin\omega_0}{r^2-a^2}\left[3\left(1-\frac{a^2}{r^2}\right)+\frac{a^4}{r^4}-2\frac{a^2}{r^2}\left(1-\frac{a^2}{r^2}\right)^2\sin^2\omega_0\right]. \tag{58}$$

5.3. Interaction and core energies for a cut along the glide plane

In the preceding analysis the strain energy within a large cylinder around the void, excluding the dislocation core, was calculated from the Gauss divergence theorem by using the cut from the surface of the void to the dislocation along the x-axis (Fig. 8(a)), because the elastic stress and strain fields (and thus the elastic strain energy) are the same for any displacement discontinuity cut from the surface of the void to the dislocation. We used the cut along the x-axis, because we had available simple expressions for the stress components along the x-axis, and thus were able to readily calculate the interaction energy U associated with that cut. The natural question is what is the interaction energy corresponding to the cut along the glide plane, where the slip is actually taking place[11] (Fig. 8(b)). To circumvent a tedious calculation of the stress components along that cut, and integration to calculate their work on the displacement discontinuity, we use the following

[11] The stress and strain fields for any two cuts from the surface of the void to dislocation are the same; only the displacement fields in the region between the two cuts differ by a rigid body translation that transmits the displacement discontinuity from one cut to another.

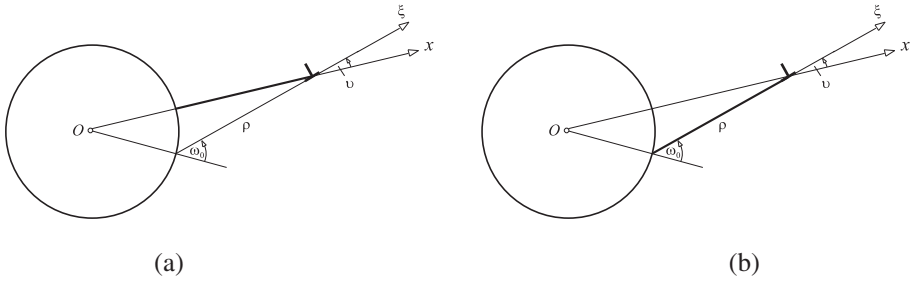

Fig. 8. A straight dislocation near a cylindrical void with the displacement discontinuity imposed from the surface of the void to the dislocation along: (a) the x-axis, and (b) the ξ-axis in the glide plane.

appealing procedure. Since the total strain energy is independent of the cut, we may write:

$$E = U + E_c = \mathbb{U} + \mathbb{E}_c, \tag{59}$$

where, from (33):

$$\mathbb{E}_c = -\frac{Gb_\rho^2(1-2\nu)}{16\pi(1-\nu)^2} \tag{60}$$

is the core energy associated with the cut along the glide plane, and $\mathbb{U}$ is the interaction energy along that cut:

$$\mathbb{U} = -\frac{1}{2}b_\rho \int_0^{\rho-c} \sigma_{n\xi}(\xi,0)\,\mathrm{d}\xi - \frac{1}{2}b_z \int_0^{\rho-c} \sigma_{nz}(\xi,0)\,\mathrm{d}\xi. \tag{61}$$

The involved resolved shear stresses are

$$\sigma_{n\xi} = -\frac{1}{2}\,(\sigma_x - \sigma_y)\sin 2\vartheta + \sigma_{xy}\cos 2\vartheta,$$
$$\sigma_{nz} = \sigma_{yz}\cos\vartheta - \sigma_{xz}\sin\vartheta. \tag{62}$$

Instead of performing lengthy calculations based on (61) and (62), we calculate $\mathbb{U}$ indirectly, from (59), as

$$\mathbb{U} = E - \mathbb{E}_c = U + E_c - \mathbb{E}_c. \tag{63}$$

Since, from (52) and (60):

$$E_c - \mathbb{E}_c = \frac{Gb_\rho^2}{4\pi(1-\nu)}\,\frac{a^2}{r^2}\,\sin^2\omega_0, \tag{64}$$

upon substitution of (50) and (64), or (54) and (60), into (63), there follows:

$$\mathbb{U} = \frac{G}{4\pi(1-\nu)}\left\{\left[b_\rho^2 + (1-\nu)b_z^2\right]\ln\left(\frac{r^2}{a^2}-1\right) + b_\rho^2\left[\frac{a^2}{r^2}\left(2-\frac{a^2}{r^2}\right)\sin^2\omega_0 - \frac{1}{2}\right]\right\}. \tag{65}$$

Fig. 9 shows the ρ-variation of U from (50), and $\mathbb{U}$ from (65). Since $\mathbb{E}_c$ is independent of ρ, the glide force is the negative gradient of the interaction energy (65) with respect to the dislocation position along the glide plane, i.e.,

$$F_\rho = -\frac{\partial \mathbb{U}}{\partial \rho}, \tag{66}$$

which reproduces (48). We recall that in the case of the cut from the dislocation to infinity (cuts type 1 from Section 5.1), the interaction energy along any such cut (along the x-axis or not) is the same, because $E_c + E_R = 0$ for each cut, so that $E = U$ and $F_\rho = -\partial U/\partial\rho$. For cuts of type 2, however, $F_\rho = -\partial E/\partial\rho = -\partial\mathbb{U}/\partial\rho \neq -\partial U/\partial\rho$.

5.4. Comparison of different glide and climb forces

To quantify the difference between the glide and climb forces associated with two types of dislocations near a cylindrical void, one emitted from the surface of the void, and the other approaching from infinity, we consider a straight dislocation in an FCC crystal, parallel to crystallographic direction $[1\bar{1}0]$, with the Burgers vector along $[011]$ direction on a slip plane $(1\bar{1}1)$; Fig. 10. By aligning the coordinate system (x_0,y_0,z), such that $x_0[110]$, $y_0[001]$, $z[1\bar{1}0]$, the Burgers vector is $\mathbf{b} = \{1,\sqrt{2},-1\}b/2$, with the magnitude $b = a_l/\sqrt{2}$, where a_l is the crystalline lattice parameter. The magnitude of the edge component of the Burgers vector, which is in the $[112]$ direction, making an angle $\vartheta_0 = 54.7°$ ($\tan\vartheta_0 = \sqrt{2}$) with the $[110]$ direction, is $b_\rho = \sqrt{3}b/2$.

Fig. 11a shows the variation of the glide force F_ρ with ρ (on the logarithmic scale), according to (42) and (48), with $\nu = 1/3$. The attraction exerted on the dislocation by the void is stronger in the case of a dislocation emitted from the surface of the void. Fig. 12(b) shows the variation of the climb force F_n, according to (43) and (49), with $\nu = 1/3$. Fig. 12 illustrates the differences between the glide and climb forces corresponding to two types of dislocations along the distance ρ/b, for two sizes of the void: $a = 10b$ and $a = 20b$. The difference between the two sets of forces is negligible far from the void, but pronounced near the void. For example, a void of radius $a = 10b$ attracts the dislocation arriving from infinity by the glide force of magnitude $0.1031\,Gb$, when the dislocation is at the distance $\rho = 2b$, while the attraction of magnitude $0.1166\,Gb$ is exerted on a dislocation emitted from the surface of the void. This means that the external loading must provide an effective shear stress on the glide plane at the center of the dislocation of the amount $\tau_{\text{eff}} = 0.1031\,G$ in the first case, and $\tau_{\text{eff}} = 0.1166\,G$ in the second case. Thus, in the analysis of dislocation emission from the surface of a cylindrical void, higher applied

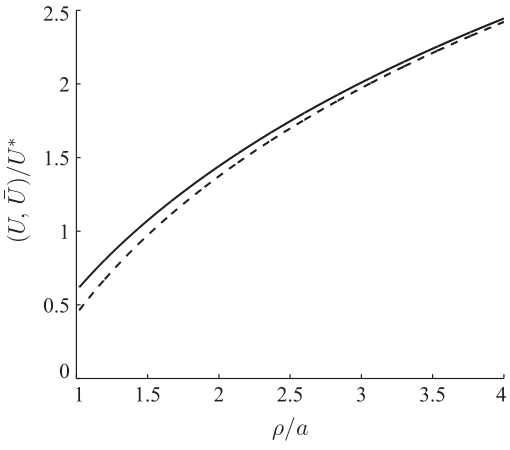

Fig. 9. The variation of the interaction energies U (dashed curve) and $\overline{U} = \mathbb{U}$ (solid curve) with ρ, according to (50) and (65). The normalizing interaction energy is $U^* = Gb^2/[4\pi(1-\nu)]$. The negative of the slope of $\overline{U}$, not U, is the glide force F_ρ.

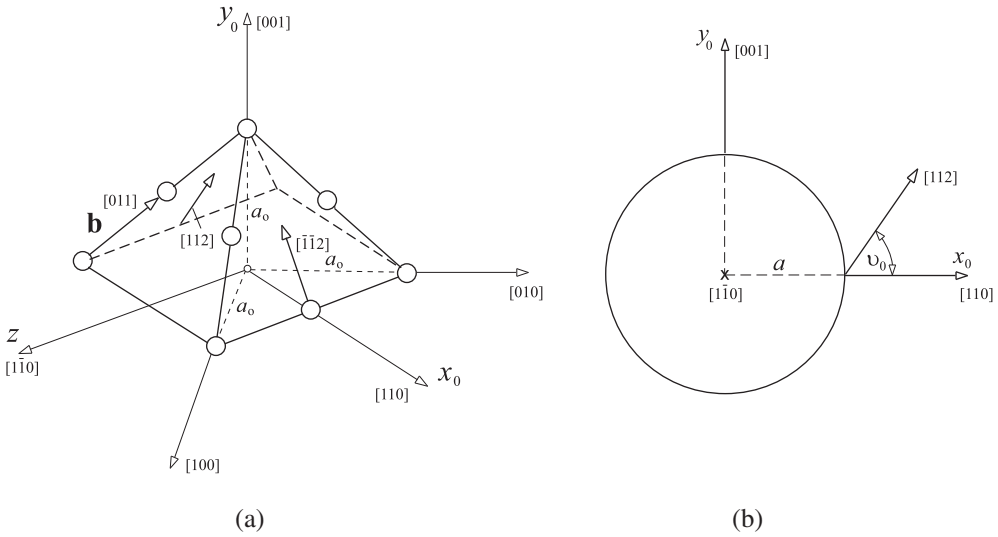

Fig. 10. (a) Four {1 1 1} slip planes in an FCC crystal, with atoms shown schematically on two of the planes only. The Burgers vector **b** of the dislocation line $[1\bar{1}0]$ is along [0 1 1] direction, with the edge component in the [1 1 2] direction. (b) The cylindrical void with the axis in the $[1\bar{1}0]$ direction. The edge component of the dislocation is along [1 1 2] direction, with tan $\vartheta_0 = \sqrt{2}$.

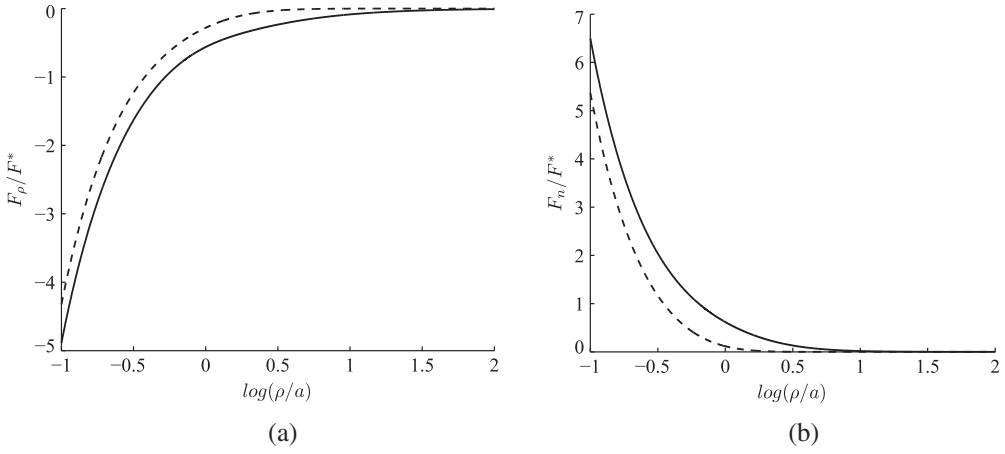

Fig. 11. The variations of the (a) glide and (b) climb forces along the slip plane corresponding to two types of dislocations located near the void. The solid curves are for the dislocation emitted from the surface of the void, and the dashed curves for the dislocation approaching the void from infinity. The scaling factor is $F^* = (Gb^2/a)/[2\pi(1-\nu)]$.

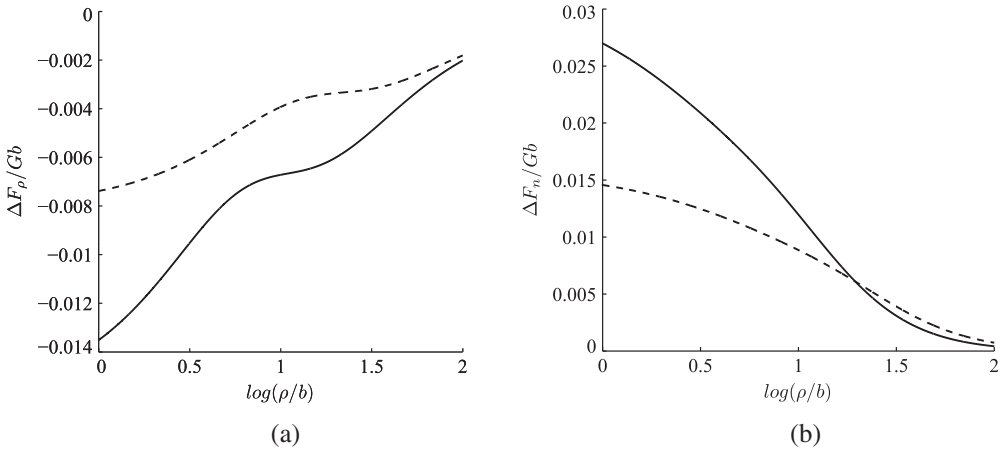

Fig. 12. The variations of the difference in the (a) glide forces $\Delta F_\rho = F_\rho^{(2)} - F_\rho^{(1)}$, and (b) climb forces $\Delta F_n = F_n^{(2)} - F_n^{(1)}$ along the slip plane corresponding to two types of dislocations. The solid curves are for the void size $a = 10b$, and the dashed curves for $a = 20b$.

stress is required to emit a straight dislocation than what was earlier predicted by using a dislocation model with the slip imposed from the dislocation to infinity (Lubarda et al., 2004; Lubarda, 2010). The effective shear stress is defined from the Peach–Koehler expression for the dislocation glide force:

$$F_\rho^{\text{ext}} = \tau_{\text{eff}} b, \quad \tau_{\text{eff}} = (b_\rho/b)\sigma_{n\rho} + (b_z/b)\sigma_{nz}, \tag{67}$$

where $\sigma_{n\rho}$ and σ_{nz} are the shear stress components from external loading at the center of dislocation in the glide (ρ) and z directions, over the slip plane with the normal n.

In the above analysis, we considered only a single dislocation with the Burgers vector $a_l[0\,1\,1]/2$ on the slip plane $(1\bar{1}1)$. The extension of the analysis to address the stress field and dislocation forces on an extended dislocation, in which the leading partial dislocation $a_l[1\,2\,1]/6$ is emitted first, leaving a faulted plane behind it, and then the trailing partial dislocation $a_l[\bar{1}12]/6$ is emitted to complete the $a_l[0\,1\,1]/2$ dislocation, is a worthwhile extension of the present analysis, particularly for FCC metals with a law stacking fault energy (such as Cu). In this case an additional length scale to consider in the analysis is a splitting distance between the partial dislocations. In BCC metals such as Mo dislocations do not split into partials and a perfect dislocation $a_l[1\,1\,1]/2$ can be considered only.

5.5. Ledge effect on a dislocation force

If the dislocation is emitted from the surface of the void, the ledge left at the surface of the void behind the dislocation can have an appreciable effect on the total force on the dislocation, increasing its attraction to the surface of the void. Adopting the Peierls model of the dislocation, the ledge force on the dislocation is Lubarda (2011):

$$F_\rho^l = -\frac{2\gamma}{\pi}\,\frac{\zeta}{\zeta^2 + (\rho/b_\rho)^2}, \quad \zeta = e^{3/2}w/(4b_\rho), \tag{68}$$

where e is the Neperian logarithm base, $w = d/(1-\nu)$ is the width of the dislocation, $d = a_l/\sqrt{3}$ is the interplanar separation across the slip plane, and γ is the corresponding surface energy. For example, for a monocrystalline copper, a reasonable estimate of γ at room temperature is $\gamma = 1.775\ \text{J/m}^2$, while the magnitude of the Burgers vector of $\{1\,1\,1\}\langle 1\,1\,0\rangle$ dislocation is $b = 0.255$ nm. By taking $G = 40$ GPa and $\nu = 1/3$, the surface energy can be conveniently expressed as $\gamma = \eta G b_\rho$, with $\eta = 0.2$. Fig. 13 shows the variation of the normalized glide force (F_ρ/Gb) on a dislocation emitted from the surface of the void vs. the normalized distance (ρ/b) along the glide plane, according to Eq. (48), i.e., without the ledge effect (solid curve), and with the added contribution (68) from the ledge. Parts (a) and (b) of the figure correspond to the void size $a = 10b$ and $a = 20b$, respectively. Evidently, while the ledge contribution to the total dislocation force is negligible at the distance ρ greater than about 10–15b, the ledge exerts a significant attraction on the dislocation in a close proximity to the void, the attraction being stronger for smaller voids. The comparison at very small ρ is, however, of little physical significance, because very near the void only an incipient dislocation resides near the void, characterized by a strongly non-linear slip discontinuity across the glide plane, and the dislocation force calculated from the Volterra dislocation model is an inadequate measure of the actual attraction exerted on the dislocation by the surface of the void.

6. Conclusion

We have derived in this paper the expressions for the glide and climb components of the image force exerted by the free surface of a cylindrical void on a nearby straight dislocation of mixed (edge-screw) type. Two different sets of these forces exist, depending on whether the dislocation has approached the void from the remote distance, or it has been emitted from the surface of the void. The expressions for the latter set of glide and climb forces have not been previously reported in the literature. They play an important role in the study of void growth in ductile materials by emission of dislocations, and in related problems of materials science. It is shown that the image forces are stronger on a dislocation emitted from the surface of the void than on a dislocation that has arrived near the void from far away, particularly for smaller voids. This implies that in the analysis of dislocation emission from the surface of a cylindrical void, higher applied stress is required to emit a straight dislocation than what was earlier predicted by using a dislocation model with the slip imposed from the dislocation to infinity. We have also shown that for a dislocation emitted from the surface of the void, the interaction energy depends on the cut used to impose the displacement discontinuity, which is not the case for the dislocation arriving near the void from infinity. The general expressions for the glide and climb forces on an arbitrarily inclined glide plane are also derived.

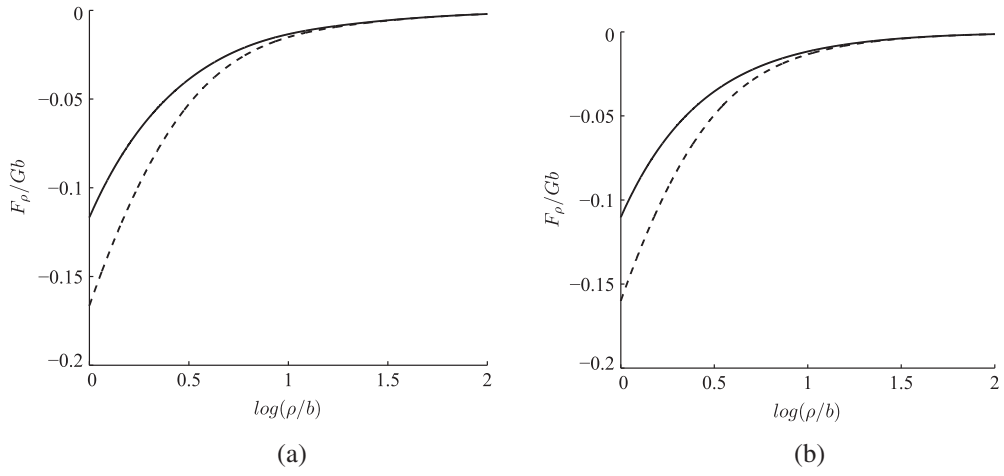

Fig. 13. The variation of the glide force with the distance from the void with the included ledge effect (dashed curve) and without it (solid curve). Part (a) is for the void size $a = 10b$ and part (b) for $a = 20b$.

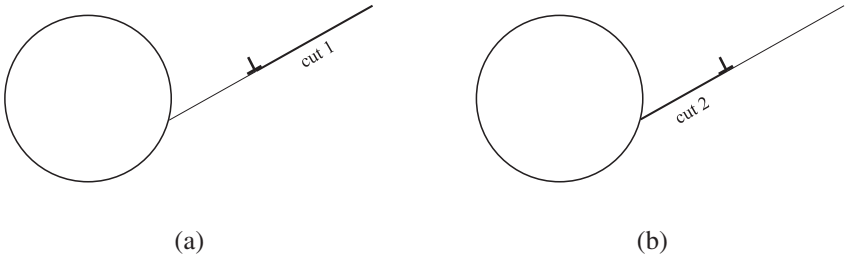

Fig. 14. A straight dislocation on its glide plane near a cylindrical void with the displacement discontinuity imposed along: (a) cut 1 and (b) cut 2.

We conclude this section by summarizing the derived expressions for the relevant (non-constant and non-divergent) portions of the elastic strain energy, and the glide and climb forces for the two types of dislocations, associated with cuts 1 and 2 (Fig. 14). For clarity, the expressions are listed separately for pure edge (b_ρ) and pure screw (b_z) dislocation components. Since there are no interaction-cross terms between the edge and screw dislocation components, their sums give the results for the general (mixed-type) straight dislocation.

Edge dislocation (Cut 1):

$$E^{(1)} = \frac{Gb^2}{4\pi(1-\nu)}\left[\ln\left(1-\frac{a^2}{r^2}\right) - \frac{a^2}{r^2}\left(1-\frac{a^2}{r^2}\,\sin^2\omega_0\right)\right],$$

$$F_\rho^{(1)} = -\frac{Gb^2}{2\pi(1-\nu)}\,\frac{a^2\cos\vartheta}{r(r^2-a^2)}\left[2-\frac{a^2}{r^2}-2\,\frac{a^2}{r^2}\left(1-\frac{a^2}{r^2}\right)\sin^2\omega_0\right],$$

$$F_n^{(1)} = \frac{Gb^2}{2\pi(1-\nu)}\,\frac{a^3\sin\omega_0}{r^2(r^2-a^2)}\left[3-2\,\frac{a^2}{r^2}-2\,\frac{a^2}{r^2}\left(1-\frac{a^2}{r^2}\right)\sin^2\omega_0\right].$$

Edge dislocation (Cut 2):

$$E^{(2)} = \frac{Gb^2}{4\pi(1-\nu)}\left[\ln\left(\frac{r^2}{a^2}-1\right)+\frac{a^2}{r^2}\left(2-\frac{a^2}{r^2}\right)\sin^2\omega_0\right],$$

$$F_\rho^{(2)} = -\frac{Gb^2}{2\pi(1-\nu)}\,\frac{r\cos\vartheta}{r^2-a^2}\left[1-2\,\frac{a^2}{r^2}\left(1-\frac{a^2}{r^2}\right)^2\sin^2\omega_0\right],$$

$$F_n^{(2)} = \frac{Gb^2}{2\pi(1-\nu)}\,\frac{a\sin\omega_0}{r^2-a^2}\left[3\left(1-\frac{a^2}{r^2}\right)+\frac{a^4}{r^4}-2\,\frac{a^2}{r^2}\left(1-\frac{a^2}{r^2}\right)^2\sin^2\omega_0\right].$$

Screw dislocation (Cut 1):

$$E^{(1)} = \frac{Gb_z^2}{4\pi}\,\ln\left(1-\frac{a^2}{r^2}\right),$$

$$F_\rho^{(1)} = -\frac{Gb_z^2}{2\pi}\,\frac{a^2\cos\vartheta}{r(r^2-a^2)},$$

$$F_n^{(1)} = \frac{Gb_z^2}{2\pi}\,\frac{a^3\sin\omega_0}{r^2(r^2-a^2)},$$

Screw dislocation (Cut 2):

$$E^{(2)} = \frac{Gb_z^2}{4\pi}\,\ln\left(\frac{r^2}{a^2}-1\right),$$

$$F_\rho^{(2)} = -\frac{Gb_z^2}{2\pi}\,\frac{r\cos\vartheta}{r^2-a^2},$$

$$F_n^{(2)} = \frac{Gb_z^2}{2\pi(1-\nu)}\,\frac{a\sin\omega_0}{r^2-a^2}.$$

Acknowledgments

Research support from the Montenegrin Academy of Sciences and Arts is gratefully acknowledged. Technical help from the undergraduate students Elizabeth Zhao and Marina Gonzales in the preparation of the manuscript is also acknowledged.

Appendix A. Stress and displacement fields of the auxiliary problem

If the uniform displacement discontinuity $\mathbf{b} = \{b_x, b_y, b_z\}$ is imposed from the surface of a cylindrical void to infinity (Fig. 2), the in-plane and out-of-plane stress and displacement components are as follows.

A.1. In-plane stress components

The stress components due to b_x and b_y are:

$$\sigma_x^{b_x} = -\frac{Gb_x y}{2\pi(1-\nu)}\,\frac{1}{r^2}\left[1+2\frac{x^2}{r^2}+\frac{a^2}{r^2}\left(1-4\frac{x^2}{r^2}\right)\right],$$

$$\sigma_y^{b_x} = -\frac{Gb_x y}{2\pi(1-\nu)}\,\frac{1}{r^2}\left[1-2\frac{x^2}{r^2}-\frac{a^2}{r^2}\left(1-4\frac{x^2}{r^2}\right)\right],$$

$$\sigma_{xy}^{b_x} = -\frac{Gb_x x}{2\pi(1-\nu)}\,\frac{1}{r^2}\left[1-2\frac{x^2}{r^2}-\frac{a^2}{r^2}\left(3-4\frac{x^2}{r^2}\right)\right],$$

and

$$\sigma_x^{b_y} = -\frac{Gb_y x}{2\pi(1-\nu)}\,\frac{1}{r^2}\left[1-2\frac{x^2}{r^2}-\frac{a^2}{r^2}\left(3-4\frac{x^2}{r^2}\right)\right],$$

$$\sigma_y^{b_y} = \frac{Gb_y x}{2\pi(1-\nu)}\,\frac{1}{r^2}\left[3-2\frac{x^2}{r^2}-\frac{a^2}{r^2}\left(3-4\frac{x^2}{r^2}\right)\right],$$

$$\sigma_{xy}^{b_y} = -\frac{Gb_y y}{2\pi(1-\nu)}\,\frac{1}{r^2}\left[1-2\frac{x^2}{r^2}-\frac{a^2}{r^2}\left(1-4\frac{x^2}{r^2}\right)\right].$$

When the stress field is recast in polar coordinates, it follows that σ_r and $\sigma_{r\theta}$, due to each b_x and b_y, are proportional to either $r^{-1}(1-a^2/r^2)\sin\theta$ or $r^{-1}(1-a^2/r^2)\cos\theta$, so that the surface of the void is traction free and the stresses vanish at infinity. The hoop stress at the surface of the void is

$$\sigma_\theta(a,\theta) = -\frac{G}{\pi(1-\nu)}\,\frac{1}{a}\,(b_x\sin\theta - b_y\cos\theta),$$

which has the maximum magnitude:

$$\sigma_\theta^{\max} = \frac{G}{\pi(1-\nu)}\,\frac{b_\rho}{a}, \quad b_\rho = (b_x^2+b_y^2)^{1/2},$$

at the angle θ defined at $\tan\theta = -b_x/b_y$. The corresponding hoop strain at those points is of magnitude $\epsilon_\theta = (b_\rho/a)/2\pi$. Thus, in order that strains are reasonably small (say, less than 2% or so), as assumed in the linear elasticity analysis, the radius of the void should be greater than about $10b_\rho$. If the slip discontinuity is b_x only, the maximum hoop stress is at $\theta = \pi/2$ (compression) and $\theta = -\pi/2$ (tension); if it is b_y only, the maximum hoop stress is at $\theta = 0$ (compression) and $\theta = \pi$ (tension).

A.2. In-plane displacement components

The displacement components due to b_x and b_y are:

$$u_x^{b_x} = \frac{b_x}{4\pi(1-\nu)}\left[2(1-\nu)\theta + \frac{xy}{r^2}\left(1-\frac{a^2}{r^2}\right)\right],$$
$$u_y^{b_x} = -\frac{b_x}{4\pi(1-\nu)}\left[(1-2\nu)\ln\frac{r}{a} + \frac{x^2}{r^2} + \frac{a^2}{2r^2}\left(1-2\,\frac{x^2}{r^2}\right)\right],$$

and

$$u_x^{b_y} = \frac{b_y}{4\pi(1-\nu)}\left[(1-2\nu)\ln\frac{r}{a} - \frac{x^2}{r^2} + \frac{a^2}{2r^2}\left(1+2\,\frac{x^2}{r^2}\right)\right],$$
$$u_y^{b_y} = \frac{b_y}{4\pi(1-\nu)}\left[2(1-\nu)\theta - \frac{xy}{r^2}\left(1-\frac{a^2}{r^2}\right)\right],$$

where $0 \leqslant \theta \leqslant 2\pi$.

A.3. Out-of-plane stress and displacement components

The out-of-plane stresses and displacement are:

$$\sigma_{zx} = -\frac{Gb_z}{2\pi}\,\frac{y}{r^2}, \quad \sigma_{zy} = \frac{Gb_z}{2\pi}\,\frac{x}{r^2},$$
$$u_z = \frac{b_z}{2\pi}\,\theta, \quad 0 \leqslant \theta \leqslant 2\pi.$$

Appendix B. Stress and displacement fields for a dislocation emitted from the surface of the void

If a straight dislocation is emitted from the surface of the void and it is in the position shown in Fig. 3, the in-plane and out-of-plane stress and displacement components are as follows.

B.1. In-plane stress components

The stress components due to b_x and b_y are:

$$\sigma_x^{b_x} = -\frac{Gb_x y}{2\pi(1-\nu)}\left[\frac{1}{r_1^2}\left(1+2\frac{x_1^2}{r_1^2}\right) - \frac{1}{r_2^2}\left(1+2\frac{x_2^2}{r_2^2}\right) + 2\,\frac{\alpha^2-1}{\alpha^3}\,\frac{ax_2}{r_2^4}\left(1-4\frac{x_2^2}{r_2^2}\right) - \frac{(\alpha^2-1)^2}{\alpha^4}\,\frac{a^2}{r_2^4}\left(1-4\frac{x_2^2}{r_2^2}\right)\right],$$

$$\sigma_y^{b_x} = -\frac{Gb_x y}{2\pi(1-\nu)}\left[\frac{1}{r_1^2}\left(1-2\frac{x_1^2}{r_1^2}\right) - \frac{1}{r_2^2}\left(1-2\frac{x_2^2}{r_2^2}\right) - 2\,\frac{\alpha^2-1}{\alpha^3}\,\frac{ax_2}{r_2^4}\left(3-4\frac{x_2^2}{r_2^2}\right) + \frac{(\alpha^2-1)^2}{\alpha^4}\,\frac{a^2}{r_2^4}\left(1-4\frac{x_2^2}{r_2^2}\right)\right],$$

$$\sigma_{xy}^{b_x} = -\frac{Gb_x}{2\pi(1-\nu)}\left[\frac{x_1}{r_1^2}\left(1-2\frac{x_1^2}{r_1^2}\right) - \frac{x_2}{r_2^2}\left(1-2\frac{x_2^2}{r_2^2}\right) + \frac{\alpha^2-1}{\alpha^3}\,\frac{a}{r_2^2}\left(1-8\frac{x_2^2}{r_2^2}+8\frac{x_2^4}{r_2^4}\right) + \frac{(\alpha^2-1)^2}{\alpha^4}\,\frac{a^2x_2}{r_2^4}\left(3-4\frac{x_2^2}{r_2^2}\right)\right],$$

and

$$\sigma_x^{b_y} = -\frac{Gb_y}{2\pi(1-\nu)}\left\{\frac{x_1}{r_1^2}\left(1-2\frac{x_1^2}{r_1^2}\right) - \frac{x_2}{r_2^2}\left(1-2\frac{x_2^2}{r_2^2}\right) + \frac{\alpha^2-1}{\alpha}\left[\frac{a}{r_2^2}\left(1-2\frac{x_2^2}{r_2^2}\right) - \frac{a}{r^2}\left(1-2\frac{x^2}{r^2}\right)\right] + 2\,\frac{\alpha^2-1}{\alpha^3}\,\frac{ax_2^2}{r_2^4}\left(3-4\frac{x_2^2}{r_2^2}\right) - \frac{(\alpha^2-1)^2}{\alpha^4}\,\frac{a^2x_2}{r_2^4}\left(3-4\frac{x_2^2}{r_2^2}\right)\right\},$$

$$\sigma_y^{b_y} = \frac{Gb_y}{2\pi(1-\nu)}\left\{\frac{x_1}{r_1^2}\left(3-2\frac{x_1^2}{r_1^2}\right) - \frac{x_2}{r_2^2}\left(3-2\frac{x_2^2}{r_2^2}\right) + \frac{\alpha^2-1}{\alpha}\left[\frac{a}{r_2^2}\left(1-2\frac{x_2^2}{r_2^2}\right) - \frac{a}{r^2}\left(1-2\frac{x^2}{r^2}\right)\right] - 2\,\frac{\alpha^2-1}{\alpha^3}\,\frac{a}{r_2^2}\left(1-5\frac{x_2^2}{r_2^2}+4\frac{x_2^4}{r_2^4}\right) - \frac{(\alpha^2-1)^2}{\alpha^4}\,\frac{a^2x_2}{r_2^4}\left(3-4\frac{x_2^2}{r_2^2}\right)\right\},$$

$$\sigma_{xy}^{b_y} = -\frac{Gb_y y}{2\pi(1-\nu)}\left[\frac{1}{r_1^2}\left(1-2\frac{x_1^2}{r_1^2}\right) - \frac{1}{r_2^2}\left(1-2\frac{x_2^2}{r_2^2}\right) - 2\,\frac{\alpha^2-1}{\alpha}\,a\left(\frac{x_2}{r_2^4} - \frac{x}{r^4}\right) + 4\,\frac{\alpha^2-1}{\alpha^3}\,\frac{ax_2}{r_2^4}\left(1-2\frac{x_2^2}{r_2^2}\right) - \frac{(\alpha^2-1)^2}{\alpha^4}\,\frac{a^2}{r_2^4}\left(1-4\frac{x_2^2}{r_2^2}\right)\right].$$

The utilized auxiliary coordinates are $x_1 = r_1\cos\theta_1 = x - \alpha a$, $x_2 = r_2\cos\theta_2 = x - a/\alpha$, and $y_1 = y_2 = y$.

B.2. In-plane displacement components

The displacement components due to b_x and b_y are:

$$u_x^{b_x} = -\frac{b_x}{4\pi(1-\nu)}\left[2(1-\nu)(\theta_2-\theta_1) + \frac{x_2y_2}{r_2^2} - \frac{x_1y_1}{r_1^2} + \frac{\alpha^2-1}{\alpha^3}\,\frac{ay_2}{r_2^2}\left(1-2\nu+\frac{2x_2^2}{r_2^2} - \frac{\alpha^2-1}{\alpha}\,\frac{ax_2}{r_2^2}\right)\right],$$

$$u_y^{b_x} = -\frac{b_x}{4\pi(1-\nu)}\left\{(1-2\nu)\ln\frac{r_1}{r_2} + \frac{x_1^2}{r_1^2} - \frac{x_2^2}{r_2^2} + \frac{\alpha^2-1}{\alpha^3}\,\frac{ax_2}{r_2^2}\left[3-2\nu-\frac{2x_2^2}{r_2^2} - \frac{\alpha^2-1}{\alpha}\left(\frac{a}{2x_2} - \frac{ax_2}{r_2^2}\right)\right]\right\},$$

and

$$u_x^{b_y} = \frac{b_y}{4\pi(1-\nu)}\left\{(1-2\nu)\ln\frac{r_1}{r_2} + \frac{x_2^2}{r_2^2} - \frac{x_1^2}{r_1^2} + \frac{\alpha^2-1}{\alpha}\,a\left(\frac{x}{r^2} - \frac{x_2}{r_2^2}\right) + \frac{\alpha^2-1}{\alpha^3}\,\frac{ax_2}{r_2^2}\left[2\nu - \frac{2x_2^2}{r_2^2} + \frac{\alpha^2-1}{\alpha}\left(\frac{a}{2x_2} + \frac{ax_2}{r_2^2}\right)\right]\right\},$$

$$u_y^{b_y} = \frac{b_y}{4\pi(1-\nu)}\left\{2(1-\nu)(\theta_1-\theta_2) + \frac{x_2y_2}{r_2^2} - \frac{x_1y_1}{r_1^2} + \frac{\alpha^2-1}{\alpha}\,a\left(\frac{y}{r^2} - \frac{y_2}{r_2^2}\right) + \frac{\alpha^2-1}{\alpha^3}\,\frac{ay_2}{r_2^2}\left[2(1-\nu) - \frac{2x_2^2}{r_2^2} + \frac{\alpha^2-1}{\alpha}\,\frac{ax_2}{r_2^2}\right]\right\}.$$

The angle range is $-\pi \leqslant (\theta_1, \theta_2) \leqslant \pi$, so that the displacement discontinuity is imposed from the surface of the void to the center of dislocation along the x-axis. The rigid body displacement $u_x^0 = c_1 + c_3 y$ and $u_y^0 = c_2 - c_3 x$ can be added as needed, where the constants c_1 and c_2 correspond to translation and c_3 to rotation.

B.3. Out-of-plane stress and displacement components

The out-of-plane stresses associated with the screw dislocation component are:

$$\sigma_{zx} = -\frac{Gb_z}{2\pi}\,y\left(\frac{1}{r_1^2} - \frac{1}{r_2^2}\right), \quad \sigma_{zy} = \frac{Gb_z}{2\pi}\left(\frac{x_1}{r_1^2} - \frac{x_2}{r_2^2}\right).$$

The out-of-plane displacement is

$$u_z = \frac{b_z}{2\pi}\,(\theta_1 - \theta_2).$$

These are the same stress and displacement fields as if the opposite screw dislocation was in a solid circular cylinder at the conjugate point $x = a/\alpha$, and the displacement discontinuity was imposed from

the dislocation to the free surface of the cylinder at $x = a$ (Eshelby, 1979).

References

Ahn, D.C., Sofronis, P., Minich, R., 2006. On the micromechanics of void growth by prismatic-dislocation loop emission. J. Mech. Phys. Solids 54, 735–755.

Asaro, R.J., Lubarda, V.A., 2006. Mechanics of Solids and Materials. Cambridge University Press, Cambridge.

Belak, J., 1998. On the nucleation and growth of voids at hight strain-rates. J. Comput. Aided Mater. Des. 5, 193–206.

Bringa, E.M., Lubarda, V.A., Meyers, M.A., 2010. Response to "shear impossibility – comments on 'void growth by dislocation emission' and 'void growth in metals'". Scripta Mater. 63, 148–150.

Bulatov, V.V., Wolfer, W.G., Kumar, M., 2010. Shear impossibility – comments on 'void growth by dislocation emission' and 'void growth in metals'. Scripta Mater. 63, 144–147.

Dundurs, J., 1969. Elastic interactions of dislocations with inhomogeneities. In: Mura, T. (Ed.), Mathematical Theory of Dislocations. ASME, New York, pp. 70–115.

Dundurs, J., Mura, T., 1964. Interaction between an edge dislocation and a circular inclusion. J. Mech. Phys. Solids 12, 177–189.

Dundurs, J., Sendeckyj, G.P., 1965. Edge dislocation inside a circular inclusion. J. Mech. Phys. Solids 13, 141–147.

Eshelby, J.D., 1979. Boundary problems. In: Nabarro, F.R.N. (Ed.), Dislocations in Solids, vol. 1. North Holland, Amsterdam, pp. 167–221.

Gavazza, S.D., Barnett, D.M., 1976. The self-force on a planar dislocation loop in an anisotropic linear-elastic medium. J. Mech. Phys. Solids 24, 171–185.

Head, A.K., 1953. The interaction of dislocations and boundaries. Philos. Mag. 44, 64–92.

Hirth, J.P., Lothe, J., 1982. Theory of Dislocations, second ed. Wiley, New York.

Lubarda, V.A., 1997. Energy analysis of dislocation arrays near bimaterial interfaces. Int. J. Solids Struct. 34, 1053–1073.

Lubarda, V.A., 1998. Dislocation arrays at the interface between an epilayer and its substrate. Math. Mech. Solids 4, 411–431.

Lubarda, V.A., 1999. On the non-uniqueness of solution for screw dislocations in multiply connected regions. J. Elasticity 52, 289–292.

Lubarda, V.A., 2003. The effects of couple stresses on dislocation strain energy. Int. J. Solids Struct. 40, 3807–3826.

Lubarda, V.A., 2006. Dislocation conditions revisited. Int. J. Solids Struct. 43, 3444–3458.

Lubarda, V.A., 2011. Emission of dislocations from nanovoids under combined loading, Int. J. Plasticity 27, 181–200.

Lubarda, V.A., Markenscoff, X., 2003. The stress field for a screw dislocation near cavities and straight boundaries. Mater. Sci. Eng. A 349, 327–334.

Lubarda, V.A., Schneider, M.S., Kalantar, D.H., Remington, B.R., Meyers, M.A., 2004. Void growth by dislocation emission. Acta Mater. 52, 1397–1408.

Meyers, M.A., Traiviratana, S., Lubarda, V.A., Bringa, E.M., Benson, D.J., 2009. The role of dislocations in the growth of nanosized voids in ductile failure of metals. J. Mater. 61, 35–41.

Moriarty, J.A., Belak, J.F., Rudd, R.E., Söderlind, P., Streitz, F.H., Yang, L.H., 2002. Quantum-based atomistic simulation of materials properties in transition metals. J. Phys. Condens. Matter 14, 2825–2857.

Rice, J.R., 1992. Dislocation nucleation from a crack tip: an analysis based on the Peierls concept. J. Mech. Phys. Solids 40, 239–271.

Rudd, R.E., 2009. Void growth in BCC metals simulated with molecular dynamics using the Fennis–Sinclair potential. Philos. Mag. 89, 3133–3161.

Rudd, R.E., Belak, J.F., 2002. Void nucleation and associated plasticity in dynamic fracture of polycrystalline copper: an atomistic simulation. Comput. Mater. Sci. 24, 148–153.

Segurado, J., Llorca, J., 2009. An analysis of the size effect on void growth in single crystals using discrete dislocation dynamics. Acta Mater. 57, 1427–1436.

Song, Z.-F., Zhu, W.-J., Deng, X.-L., He, H.-L., 2006. Crystal-orientation dependent evolution of edge dislocations from a void in single crystal Cu. Chin. Phys. Lett. 23, 3041–3044.

Tadmor, E.B., Ortiz, M., Phillips, R., 1996. Quasicontinuum analysis of defects in solids. Philos. Mag. A 73, 1529–1563.

Traiviratana, S., Bringa, E.M., Benson, D.H., Meyers, M.A., 2008. Void growth in metals: atomistic simulations. Acta Mater. 56, 3874–3886.

Willis, J.R., Bullough, R., 1971. The interaction between a void and a dislocation loop. In: Pugh, S.F. (Ed.), Proceedings of the BNES European Conference on Void Formed by Irradiation Reactor Materials. Reading University, pp. 133–147.

Wolfer, W.G., Drugan, W.J., 1988. Elastic interaction between a prismatic dislocation loop and a spherical cavity. Philos. Mag. A 57, 923–937.